Multispectral maritime background and clutter effects on small surface target detection

Arie de Jong

TNO Physics and Electronics Laboratory
PO Box 96864, 2509 JG The Hague, The Netherlands

ABSTRACT

This paper concerns multispectral backgrounds and clutter as they hamper the detection process of small surface targets. The variability of target contrast is shown for a number of meteorological conditions in the various spectral bands, for which new types of sensors have become available. It is shown that simultaneous framing with pixel co-location is very essential, which requires automatically the application of staring 2-D arrays. Some additional sensor tricks are introduced such as gated viewing, dynamic range enhancement, and laser 3-D imaging. By proper selection of bands, optimum clutter reduction and detection probability can be achieved for targets such as swimmers, buoys and zodiacs.

Keywords: Maritime backgrounds, Multispectral target detection, Clutter, Electro-Optics and Infrared.

1. INTRODUCTION

The detection of small maritime surface targets is a topic of growing importance, especially for operations in coastal areas. The type of targets can be of various nature: buoys, floating mines, swimmers, drowned persons, small inflatable boats, periscopes etc. The application can be military or civil, rescue or warning, surveillance or area control. In many cases the radar cross section of these targets is very low and radar returns suffer from clutter due to wave structures and low doppler contributions due to the low target speed.

Detection by electro-optical and infrared means offers the advantage of higher spatial resolution and possibilities of sensor fusion at the pixel level. Furthermore, if the full EO/IR spectral band is covered, target contrast is dominated from a reflective picture in the visual and near IR towards a primarily emissive picture in the Long Wave (LW) IR band, showing differences in apparent temperature.

Although the reflecting properties of the water surface are not that much varying with wavelength and the target surface reflectance can be spectrally indifferent, still target contrast differences can be found in the various spectral bands. This is caused by the reflection of the sky background from the sea surface. This sky background contributes negatively in the LWIR and positively in the visual (day time). Therefore, LWIR target contrast is positive in flat sea conditions most of the time, even when the water, air and target temperatures are the same. In the visual the contrast is negative most of the time, when the surface reflectance is low (black). This is the most pronounced when the target is located in sun glint directions.

In less ideal conditions such as nighttime, poor visibility, complete and low cloud cover, rain and snow and higher sea states, complications are occurring that hamper the detection process. Especially when the time for target detection is limited because the sensor package is mounted in an airborne platform and large areas have to be surveyed in a short time period.

It has to be mentioned that this surveillance circumstance is the worst possible. Stationary coastal platforms allow frame to frame correlation techniques, suppressing clutter by means of temporal algorithms. Sensors on board of ships, or mounted in periscopes from submarines, suffer also from irregular motions of the platform. However, just these motions may allow for algorithms based upon the variations in observation direction to the target. In this way perspective algorithms are available to find the target, although the variations in the clutter structure with time are a limiting factor.

This paper will concentrate on new sensors and techniques which have become available for small maritime target detection and their capabilities against these targets. An analysis will be presented on the target contrast in various conditions, followed by a review of the problems, especially the false alarms. In a discussion the status of the activities at TNO-FEL will be presented as well as a review on optimum sensor band combinations.

0-8194-2123-5/96/$6.00

2. SENSOR OPPORTUNITIES

For multispectral detection techniques the ideal situation is that the object space is imaged by the sensor package with the sensor entrance pupils at the same place. Furthermore, pixels in the various sensors should be co-located and the frames should be taken time synchronous. These requirements involve quite a lot of techniques such as dichroic beam splitters, distortion free lens systems, identical Instantaneous Fields of View (IFOV) and synchronized framing.
This latter aspect was a problem with IR sensors using serial-parallel scanning techniques. In those systems it is very difficult to realize that a certain pixel is observed within a few msec accuracy. Furthermore, the detector is sampling the pixel only for a very short time of a few μsec, whereas staring sensors average over a number of msec. It is also very difficult in these sensors to achieve that the IFOV of a pixel is identical to that of a staring sensor. Finally the sensors with mechanical scanning most of the time suffer from distortion, which means that towards the edges of the field of view the pixels are not co-located. In the distortion correction algorithms errors are introduced, resulting from spaces between detector elements and non-equal point spread functions.

However, in the last decade full staring sensors have become available from the UV to the LWIR allowing improved multispectral sensing techniques. Following is a list with examples of materials involved with the sensors.

- Silicon, UV enhanced for the spectral region 0,35-0,40 micrometer. Detector arrays of 640×480 elements are available. To solve the problem of lack of sensitivity because of the fact that the scene brightness is lower than in the visual band, improvement can be obtained by thermo-electrical cooling of the chip or in the ultimate case by including a Micro Channel Plate (MCP) intensifier with S25 cathode.
- Silicon for the visual band (0,4-0,7 micrometer). Because of the availability of sufficient scene brightness subbands can be used. Narrow band (0,01 micrometer) imaging can be used by applying cooling or image intensification as with the UV sensor. Another advantage of cooling is the increase of the dynamic range to more than 12 bits. Color camera's with 3 co-located chips are available to take red, green and blue images. The advantage of this spectral band is the low cost of the sensors because of the wide civil application.
- Silicon for the near IR (0,7-1,0 micrometer), the spectral band where the detector response has its maximum. For this band the atmospheric scattering is definitely lower than in the visual, which provides a typical advantage. By again applying an MCP the sensitivity can be increased for obtaining nighttime imagery. Also in this region laser target illumination can be applied, resulting in possibilities for ranging and background irradiance with dark targets at short range. In the case the MCP is appropriately gated.
- Indium gallium Arsenide (1,0-1,7 micrometer); in this spectral band with better atmospheric propagation than the previous band, the spectral reflectance properties of several materials are completely different from the 0,7-1,0 μm band. Arrays of 128×128 have been realized, which means that compared to a 512×512 array we have to integrate over 4×4 pixels or reduce the field of view with a factor 4.
- Platimum Silicide (2,0-2,6 and 3,4-4,1 micrometer). This detector material has proved its capability and arrays of 512×512 and more have been produced. The disadvantage of lower quantum efficiency is compensated by the very good uniformity and low cost, also for the read-out. A disadvantage is the required cooling to below 80K, although cheap, low power and reliable coolers are available these days. The spectral band of 2,0-2,6 μm in the range where solar irradiance is becoming drastically smaller and thermal contrast is very low. The spectral band 3,4-4,1 μm however, is perfect for thermal detection, because the atmosphere is very clear in this band.
- IndiumAntimonide (3,4-5,3 micrometer). This classical detector material has been produced in arrays of up to 512×512 detectors. The quantum efficiency is good but detector non-uniformities require adequate correction algorithms. Especially when this sensor is used in a multispectral snesor package, frequent calibration is required. The spectral part between 4,5 and 5,3 micrometer is of less use for targets at longer ranges because of high atmospheric absorption/emission in higher humidity conditions.
- Mercury Cadmium Telluride (3-5 and 8-10 micrometer); for the 3-5 μm band thermo-electric cooling up to higher temperatures (190K) is sufficient, but the 8-10 μm detector needs an operating temperature of 80K. Arrays of 256×256 elements have been realized. Even more than InSb this detector requires very good non-uniformity correction, due to the easily present crystal inhomogeneities (composition). For the 10 μm band 128×128 element arrays are available. This band is ideal because it is the center of thermal emission of 300K targets.
- GaAs; GaAlAs Multi Quantum Well (around 9 micrometer); the spectral band of these detectors is selectable in accordance with the material composition. Arrays of 128×128 have been manufactured and the sensitivity is comparable to MCT (about 0,05K). This new material is not yet widely available and rather expensive.

- Uncooled arrays (3-14 micrometer) either silicon bolometric or BaSr (TiO_4) or other ferro-electric materials are becoming better and cheaper. Arrays of more than 256x256 elements have been realized. Their sensitivity goes up to 0,1K in the 8-14 μm band, which make them attractive in certain applications. Because of the high speed optics, for high spatial resolution, big optical elements are required.
- Sandwich detectors (visual/IR) have been realized since a long time for single elements. For 2-D arrays manufacturing problems increase but seem to be solvable, for example with materials like Si:Ge. In the ideal situation a package of 3-4 arrays, of which the top one is sensitive in the shorter spectral band and the bottom one in the longer spectral band, will become available. This wide spectral band solution (including mirror-optics) allows for perfect imaging through one single entrance pupil.
- Imaging spectrometers (wide band); these sensors are under development now and provide high spectral resolution (hyperspectra). A disadvantage is that it takes some time to make an image, reason why these devices are not suitable for all applications (flying and sailing) when very precise platform stabilization is not available. Another disadvantage is that they are not fitting to other 2-D imaging techniques.
- Laser 3-D imaging (0,8; 1,06; 1,54; 10,6 micrometer). Different from the laser gated viewing in combinations with the MCP this technique uses a scanning laser beam in 2-D, where the 3rd dimension (range) is obtained by appropriate pulsing. The field of view will be small in general (e.g. 32x32 pixels) and the technique can be used for target identification and false alarm reduction.The advantage is that due to the retro-effect, EO/IR sensors on the target will appear brightly. It is clear that the laser wavelengths mentioned, in combination may provide multispectral capability.
- Polarization filters are available for all spectral bands. In a certain spectral band the target contrast can be different for the polarization direction parallel to the plane of incidence compared to the polarization direction perpendicular to the plane of incidence. For flat sea surfaces and higher elevation angles the effect becomes bigger with a maximum for the brewster angle, which occurs for an elevation angle of about 35°.

3. TARGET CONTRAST

As mentioned in the introduction only the contrast of small targets will be considered here in the various spectral bands. We take a floating cilinder with diameter and height above the water of 1m. So the perceived size in flat sea conditions is $1m^2$ for all directions. We will assume the target to be painted with a perfectly diffuse paint with spectral emissivity $\varepsilon(\lambda)$ between black and white. The geometry is illustrated in fig. 1 where φ is the look-down angle, defined by the range R and sensor height h.

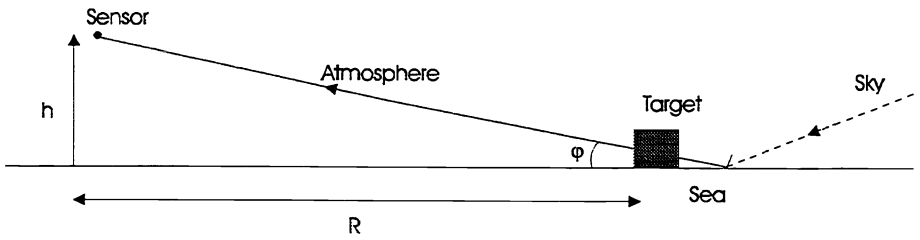

Fig. 1. Geometry of Target observation by Multispectral Sensor.

Because of the tremendous variability of the target contrast, we will only consider here some relevant conditions but cover both the reflective and emissive contrast and demonstrate the power of spectral band combination. We will make the following assumptions and conditions:

- ignore polarization effects
- the air temperature equals the water temperature
- the target has a temperature 2°C above the air temperature
- the target has a variable emissivity between 0,3 and 0,9 in the 3-14 μm bands
- the target has an emissivity between 0,2 and 0,8 in the 0,3-3 μm bands
- the visibility is 20 km; water vapour: 5 g/m^3 at sea level
- the sea surface is flat or ruffled
- for look-down angle we take 0,5° and 5°
- the sky is clear or overcast with cloud temperature T_{air}-6°C
- sunglint is excluded
- we take midlatitude daytime condition, springtime or fall.

The most dominant factor in maritime target contrast is not so much the target itself but the radiation from the sea background. The optical properties of sea water are well known[1] and as a result the reflectivity of a flat water surface can be calculated easily by means of Fresnel's formula. The result is shown in fig. 2 for down look angles between 0° and 10°. Although the curve is calculated for wavelength of 5 μm and the complex index of refraction of water is wavelength dependent, the curve is representative as an average for all spectral bands from visual to IR[2].

We observe that for down look angles between 0° and 5° more than 60% of the perceived radiance is reflected sky radiance for a flat sea.

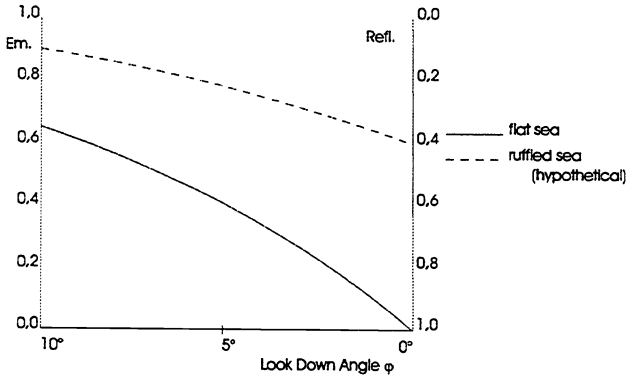

Fig. 2. Emissivity and Reflectivity of Sea Water as function of Look Down Angle.

Sky radiance in itself is a function of elevation angle[3] , especially for clear sky conditions in the LWIR. As a result total LWIR has been verified experimentally by year round measurements[4]. The effect of surface roughness on background radiance has been modelled recently by Zeisse[5]. Typical radiance plots are shown in fig. 3 and fig. 4.

We will present target contrast for 5 of the 7 spectral bands of interest in terms of radiance difference at zero range. For the sake of simplicity we compare the resulting contrast with the sensitivity levels of the sensors in chapter 2. For example, in the thermal bands the temperature resolution is better than 0,1K. When target contrast is between 0,1 and 1K, we nominate a +, between 1K and 3K a ++ and for larger contrasts we put +++. For negative contrasts we put resp -, -- and ---. These contrast categories are intentionally somewhat rough, because detailed numbers are not needed for this study of spectral band comparison for the variable scenarios we take.

In a similar way we operate in the visual and Near IR bands in comparison with the sensor noise levels. The resulting table gives a good insight in the bands to choose for a given condition. Table 1 shows the results for the condition of the target temperature being 2° above air temperature T_{air} and a near black target (ε = 0,9) for all spectral bands. Of course in the end the atmospheric absorption has to be considered; especially for lower visibility conditions, preference appears for the longer wavelengths.
Values in the table can be obtained by means of the formula:

$$C(\varphi) = \varepsilon_t N_t + (1-\varepsilon_t)\left(\tilde{N}_{sky} + \tilde{N}_{sea}\right) - \varepsilon_s N_{sea} - (1-\varepsilon_s) N_{sky} \qquad (1)$$

where C(φ) is the radiance difference in ratio to the sensor noise level, ε_t the target emissivity, N_t the target radiance (0 in visual, NIR), $\tilde{N}_{sky}$ the sky radiance as reflected by the target for a vertical surface, $\tilde{N}_{sea}$ the sea radiance as reflected by the target, ε_s the sea emissivity from fig. 2, N_{sea} the sea radiance, which may be partly skylight entering into the sea and scattered back, N_{sky} the sky radiance according to fig. 3 and 4. It is approximated here that the ruffled sea reflects the average sky radiance between 0° and 30° elevation angles.

While table 1 just shows positive contrast for the thermal bands and generally negative contrast for the visual/NIR, table 2 gives more differentiation in the visula/NIR bands, due to the variable target emissivity. For these bands we can simplify formula (1) to:

$$C(\varphi) = \left[\alpha(1-\varepsilon_t) - \beta(1-\varepsilon_s)\right] N_{sky} \qquad (2)$$

where α and β are condition dependent parameters. We take for them α = 0,6; 0,4 resp. 0,5 and β = 1; 1; 0,8 and 1,2 for flat/clear, flat/overcast, ruffled/clear resp. ruffled/overcast conditions.

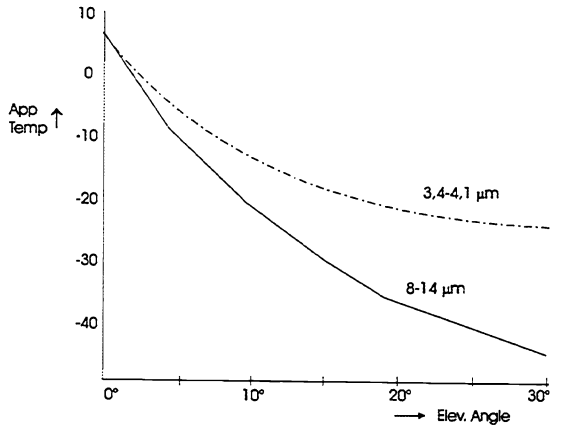

Fig. 3. Lowtran calculation of Apparent Temp as function of Elevation Angle (from[4])

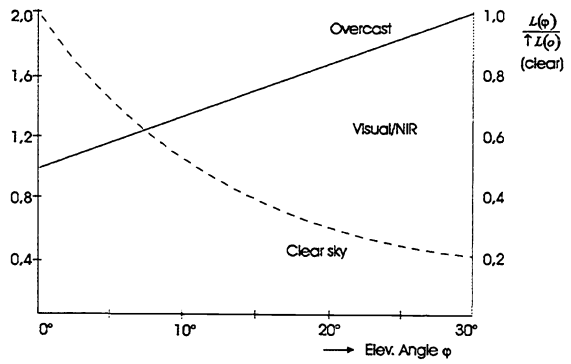

Fig. 4. Cloud radiance as function of Elevation Angle; Overcast Sky ——— and typical Clear Daytime Sky ------- $L(\varphi)$ = radiance for elevation angle (from[3])

Conditions			Spectral Band (µm)				
Sea	Sky	Down Look Angle	0,4-0,7	0,7-1,0	1,0-1,7	3,4-4,1	8-12
flat	clear	0,5°	---/---	---/---	---/-	++	++
flat	clear	5°	--/--	--/--	---/+	+++	+++
flat	overcast	0,5°	---	---	---	++	++
flat	overcast	5°	--	--	--	++	++
ruffles	clear	0,5°	-/0	-/0	0/0	+++	+++
ruffles	clear	5°	-/+	-/++	+/++	+++	+++
ruffles	overcast	0,5°	--	--	-	+++	+++
ruffles	overcast	5°	-	-	0	++	++

Table 1. Target radiant contrast for Target Emissivity $\varepsilon_t = 0{,}8$ for $\lambda < 1$ µm; $\varepsilon_t = 0{,}5$ for 1 µm $< \lambda < 3$ µm; $\varepsilon_t = 0{,}9$ for $\lambda > 3$ µm. Note: For clear conditions a/b contrast are for shadow/sunlit side of target.

Conditions			Spectral Band (µm)				
Sea	Sky	Down Look Angle	0,4-0,7	0,7-1,0	1,0-1,7	3,4-4,1	8-12
flat	clear	0,5°	--/++	--/-++	---/-	-	-
flat	clear	5°	-/+++	-/+++	--/+	+++	+++
flat	overcast	0,5°	--	--	---	+++	+++
flat	overcast	5°	-	--	--	++	++
ruffles	clear	0,5°	+/+++	+/+++	0/++	++	+++
ruffles	clear	5°	++/+++	++/++ +	+/++	++	++
ruffles	overcast	0,5°	0	0	-	++	++
ruffles	overcast	5°	+	+	0	+	+

Table 2. Target radiant contrast for Target Emissivity $\varepsilon_t = 0{,}2$ for $\lambda < 1$ µm; $\varepsilon_t = 0{,}5$ for $1 < \lambda < 3$ µm; $\varepsilon_t = 0{,}5$ for $\lambda > 3$ µm.

Conditions			Spectral Band (μm)				
Sea	Sky	Down Look Angle	0,4-0,7	0,7-1,0	1,0-1,7	3,4-4,1	8-12
flat	clear	0,5°	---/---	--/+	--/+	--	-
flat	clear	5°	--/-	-/++	-/++	+++	+++
flat	overcast	0,5°	---	---	---	--	+
flat	overcast	5°	--	-	-	++	++
ruffles	clear	0,5°	-/0	0/+++	0/+++	+	+++
ruffles	clear	5°	-/+	+/+++	+/+++	-	+++
ruffles	overcast	0,5°	--	-	-	+	++
ruffles	overcast	5°	-	0	0	-	++

Table 3. Target radiant contrast for Target Emissivity $\varepsilon_t = 0,8$ for $\lambda < 0.7$ μm; $\varepsilon_t = 0,3$ for 0,7 μm $< \lambda <$ 6 μm; $\varepsilon_t = 0,7$ for $\lambda >$ 6 μm.

Conditions			Spectral Band (μm)				
Sea	Sky	Down Look Angle	0,4-0,7	0,7-1,0	1,0-1,7	3,4-4,1	8-12
flat	clear	0,5°	--/++	---/--	---/--	0	--
flat	clear	5°	-/+++	--/-	--/-	+++	+++
flat	overcast	0,5°	--	---	---	+	--
flat	overcast	5°	-	--	--	++	+
ruffles	clear	0,5°	+/+++	-/+	-/+	+++	++
ruffles	clear	5°	++/+++	0/+	0/+	++	+
ruffles	overcast	0,5°	0	--	--	++	+
ruffles	overcast	5°	+	-	-	++	-

Table 4. Target radiant contrast for Target Emissivity $\varepsilon_t = 0,2$ for $\lambda < 0,7$ μm; $\varepsilon_t = 0,7$ for 0,7 μm $< \lambda <$ 6 μm; $\varepsilon_t = 0,3$ for $\lambda >$ 6 μm.

The 0, +/-, ++/-- and +++/--- signs in table 1 correspond to $|C(\varphi)|$ values of $< 0,1\ N_{sky}$; $0,1 < |C(\varphi)| < 0,3$; $0,3 < |C(\varphi)| < 0,6$ and $|C(\varphi)| > 0,6\ N_{sky}$. When direct sunlight irradiates the observed side, the contrast is becoming more positive for the clear conditions, as indicated in the table, due to the fact that α becomes bigger (1,6 and 1,4 instead of 0,6 and 0,4).

For the thermal bands formula (1) has been simplified to:

$$\Delta T(\varphi) = 7\varepsilon_t - 5 + \left(10/15\right)\cdot\left(1-\varepsilon_s\right) \quad \text{resp.} \quad \Delta T(\varphi) = 5\varepsilon_t - 3 + 6\left(1-\varepsilon_s\right) \qquad \text{(3) resp. (4)}$$

for clear resp. overcast conditions. The symbol (10/15) in formula (3) means that we take for clear sky, ruffled sea an average temperature jump of 10K resp. 15K for the MWIR resp. LWIR. For a flat sea we take 1K resp. 13K for look down angles of 0,5° resp. 5° (see fig. 3).

Tables 3 and 4 give similar data for other emissivities. Because of daytime imagery we have taken the target temperature 2° higher than air temperature; for nighttime the target may be a few degrees cooler than the air due to radiative cooling. The tables 1-4 show the variability of target contrast, as confirmed by experience. They also show the complementarity of each of the bands in the various conditions.

4. COMPLICATIONS BY CLUTTER

In the assumptions, we took before, local fluctuations in background radiance were not considered as sources of false alarms. In reality however, for sea states higher than 1, we have to consider them and try to find solutions to reduce these false alarms, primarily by multispectral correlations. It is interesting to observe the increased literature on sea surface modelling and EO/IR imagery of the waved surface structure.

Lévesque[6] produced the first simulated IR sea imagery, taking into account motion of the waves. Davis[7] at Areté Associates developed the IRST model IR-Tool with a strongly improved simulation methodology. More recently Constantikes[8] published a realistic clutter model with improvements in the Cox & Munk wave facet model. One of the problems for detecting small floating targets is the occlusion of the target by wave tops at shorter distance to the observer. At NRL, Takken et al[9] have carried out work on the magnitude of this effect, which has a strong statistical nature. Especially the big waves from ocean swell are good target hiders.

This effect urges the observer to take long time for surveillance, because of the time constant of swell (5-15 sec), or to move the sensor to higher altitude. In the ideal (stationary) situation he has several minutes of observation time and the target is not moving too fast, so he can observe the target several times when he is on top of a wave. In the worst case the target is moving in a wave valley with the same speed as the waves: he is constantly occluded.

In a rougher sea also wave slopes are getting bigger and angles of incidence of 60° and less are becoming common. This means an increase in the number of dark patches in the visual and "warm" (white) patches in the thermal IR, because the bright, cold sky is much less reflected (about 5% instead of 60% for 85° angle of incidence).

In the ultimate situation the wave is rolling over and a whitecap is generated. Monahan[10] carried out work on the statistics of whitecapping as function of wind speed. In this case both the visual and IR contrast of the whitecap is positive, leading to an algorithm to overcome this source of false alarm. White caps tend to be horizontally extended, which behaviour allows the use of spatial filtering techniques.

Another category of clutter is solar glint (e.g. Mermelstein[11]). Originally used by Cox & Munk to characterize the wave structure, solar glint causes many daytime problems in clear sky, or partly clouded and windy conditions, which tend to occur very frequently. In general the average background radiance is tremendously increased in all visual and NIR bands up to the MWIR, especially in the direction of the sun and a reflected sun beam in the water. The 10 μm band however, shows a minor solar glint effect. Furthermore, in more open ocean conditions, sun glints may occur 360° around. Nearly each of the surrounding waves may have a facet, which temporally reflects sun radiation towards the observer, especially for sun positions in near zenith condition.
The magnitude of these clutter phenomena, including "false alarms" such as birds and pieces of rocks, has been measured during various measurement campaigns. Both for the visual and IR peak to peak contrasts in the range of "+++" in tables 1-4 have been found. This means that in certain occasions hundreds of alarms may be present in one image, especially with solar glints.

Frame to frame correlation will reduce most of the glints due to the fact that they persist only for a short time. Again the fact that the glints have a very strong positive contrast in the visual, NIR and MWIR (3,4-4,1 μm) leads to a good discrimination capability, under condition that all camera's are perfectly synchronized.

A problem with solar glint is the overload, it can cause in the sensor, especially in the visual. This makes it necessary to reduce the exposure time, which also reduces the target contrast.

In nighttime, moonglint has a similar appearance as sunglint. When image intensification is used to obtain sufficient target contrast, similar background and clutter effects are determined as well as the methods to solve the false alarm problems.
Of course, part of the sunglint or moonglint false alarms can be reduced or eliminated by using a polarization filter, especially for the larger angles of incidence (between 20° and 40°).

In summary we may characterize the various clutter phenomena as in table 5 where the contrast is presented for various bands and also behaviour such as extension, time persistance, effect on the water surface, and displacement. From this table appropriate algorithmic techniques can be derived.

Clutter phenomena	contrast				persistance	extension	surface effect	displacement
	VIS	NIR	MWIR	LWIR				
tilted wave	---	---	+	+	10-60 sec	may be	no	yes
sunglint	+++	++	+	0	short	no	no	no
white cap	++	+	+	++	10-60 sec	may be	no	yes
bird	+/-	+/-	+	++	may be long	no	no	yes
rock	-	-	+	+	long	may be	yes	no

Table 5. Summary of clutter characteristics (false targets).

5. DISCUSSION

In chapters 3 and 4 we have seen the complications in target contrast and background cluttter for a number of conditions. The contrast tables show plenty of positive or negative contrast, depending on target emissivity and background condition. Although the UV and 2,3 μm bands were not considered, they show similar behaviour with less signal to noise ratio due to fewer solar irradiance.

The question is now which bands to combine for optimum target detection results. This optimum includes the best detection probability, the lowest false alarm rate for the least cost. An attempt to this is made in the matrix of table 6.

Of course, one has to keep in mind the application: which target has to be detected in what background from which platform with what types of false alarm causing clutter, as presented in table 7.

Sensor	approx. cost	image perf.	1	2	3	4	5	6	7	8	9	10	11	12
1. UV 0,35-0,4	20 K$	+					0				0			
2. UV enhanced	50	++						×				×		×
3. VIS 0,4-0,7	5	+					0				0			
4. VIS enhanced	50	++							×				×	×
5. NIR 0,7-1,0	5	++	0							0	0			
6. NIR enhanced	50	+++		×								×		×
7. NIR 1,0-1,7	80	+			0					0	0			
8. MWIR 2,0-2,6	60	+	0				0				0			
9. MWIR 3,4-4,1	60	++			0		0		0					
10. Enh. InSb 2-5	150	+++				×							×	×
11. LWIR 8-12	150	++				×		×				×		
12. Laser Sensor	150	+						×			×		×	

Table 6. Review matrix of sensors and some possible best 3 combinations 0 low budget
× high budget.

Target	**Background**	**Clutter**	**Sensor platform**
swimmer	daytime, clear, low sea state	birds	coast
buoy	daytime, clear, high sea state	wreckage	ship
periscope	nighttime, clear, cold	whitecap	periscope (sub)
snort	daytime, warm, humid	titled wave	uav
zodiac	coastal area, rocks, dunes	sunglint	helicopter
mine	daytime, overcast, low sea state	piece of rock	mar. patr. aircr.
drowned person	nighttime, overcast, high sea state	"occlusion"	

Table 7. List of targets, backgrounds and clutter.

We will consider 2 attractive combinations of "fused sensors". The first uses sensors 4, 6, 10, 11 and 12 from table 6. This is a "high budget" package.

The enhanced visual sensor could use a cooled CCD with high dynamic range to tackle the sunglint problem, one could provide a polarizer and the possibility exists to increase frame rate and to apply the principle of kinematic ranging (pseudo stereo). The enhanced NIR uses a gated MCP for ranging and contrast improvement. The returned signal may be increased by retro-effects (periscope). The enhanced InSb consists of a couple of InSb arrays with a dichroic, selecting 2 spectral subbands in 3-5 μm. The LWIR sensor is the basic sensor providing the best contrast day and night. The laser sensor provides an image of a limited field of view to confirm the alarm, to measure its range and eventually vibration spectrum for identification.

The second combination uses sensors 3, 5, 7 and 10, which is a "low budget" package. It is the combination we have at the moment at TNO-FEL. In confirmation with tables 1-4 these sensors are reasonably complementary. The MWIR sensors have a resolution of 0,1 mrad; the NIR we have provided with a 300 mm lens providing 20 μrad resolution, the visual camera is a 3 color RGB camera. The InGaAs camera is provided with a zoomlens. This system is used to build up a database with all possible items from table 6. Some of the imagery will be shown at the conference.

6. REFERENCES

1. The Infrared Handbook, Office of Naval Research, Washington DC, Chapter 3.7.5, marine backgrounds (1985).
2. K.T. Fosseide, "Model for calculation of IR spectral contrast in marine environments", Infrared Technology XVII, SPIE Proceedings Vol. 1762, p.251-265, (1993).
3. The Infrared and Electro Optics Handbook, Vol. 1, Sources of Radiation, Chapter 3.6, "The Sky", SPIE Optical Engineering Press, 1993.
4. J.B. van de Vrie, "Infrared Sea and Sky Background Radiation", TNO-FEL report no. PHL 1976-41, November 1976.
5. C.R. Zeisse, "Radiance of the Ocean Horizon", J. Opt. Soc. Am. A, Vol. 12, No. 9, September 1995.
6. M.P. Lévesque, "Generation of Synthetic IR Sea Images" SPIE conference on Characterization, Propagation and Simulation of IR Scenes, SPIE Proceedings, April 1990, Orlando.
7. P. Davis e.a., "Simulation and Data Analysis of Infrared Ocean Clutter at Grazing Angles", SPIE Proceedings, On Backgrounds, Orlando, April 1993.
8. K.T. Constantikes, "Modelling and Synthesizing Infrared Ocean Clutter", John Hopkins APL Techn. Digest, Vol. 16, No. 2, 1995.
9. E.H. Takken, "Observation of IR Source at Ocean Horizon", Proceedings of 1995 meeting of the IRIS Specialty Group on Targets, Backgrounds and Discrimination, ERIM, Ann Arbor, January 1995, pp.229-252.
10. E.C. Monahan, "Optimum Power Law Description of Oceanic Whitecap Coverage Dependence on Wind Speed", J. of Phys. Oceanography, Vol. 10, p.2094-2098, 1981.
11. M.D. Mermelstein, "Infrared radiance and solar glint at the ocean-sky horizon", Appl. Optics, Vol. 33, No. 25, 1 September 1994.